

Quantum State Preparation with Resolution Refinement

Scott Bogner,¹ Heiko Hergert,¹ Morten Hjorth-Jensen,² Ryan LaRose,³ Dean Lee,¹ and Matthew Patkowski⁴

¹*Facility for Rare Isotope Beams and Department of Physics and Astronomy,
Michigan State University, East Lansing, Michigan 48824, USA*

²*Department of Physics and Center for Computing in Science Education, University of Oslo, N-0316 Oslo, Norway*

³*Department of Computational Mathematics, Science,
and Engineering; Department of Electrical and Computer Engineering; Center for Quantum Computing,
Science, and Engineering; Department of Physics and Astronomy,
Michigan State University, East Lansing, MI 48824, USA*

⁴*Department of Physics, University of Colorado Boulder, Boulder CO 80309, USA*

We introduce a method called resolution refinement that allows one to bootstrap eigenstate preparation on a quantum computer. We first prepare an eigenstate of a low-resolution Hamiltonian using any method of choice. The eigenstate is then lifted to higher resolution and adiabatically evolved to produce the corresponding eigenstate of a higher-fidelity Hamiltonian. We give examples of resolution refinement applied to both single-particle basis states as well as a spatial lattice grid. For basis refinement, we compute few-body ground states of the Busch model for interacting particles in a harmonic trap in one dimension. For lattice refinement, we compute Hartree-Fock nuclear states for a central Woods-Saxon potential in three dimensions, and we compute bound states and continuum states in a multi-species Hubbard model of fermions in one dimension. In all cases, the method is efficient and requires an adiabatic evolution time comparable to the inverse of the energy gap in the physical spectrum.

A central challenge for studying quantum many-body systems on a quantum computer is the efficient preparation of complex and correlated ground states. This is a task for which many prominent algorithms face difficult scaling limits as the system size increases. Variational methods such as variational quantum eigensolvers [1] can face the challenge of exponentially vanishing gradients for large systems [2]. The runtime for adiabatic state preparation increases exponentially with system size if the initial and final Hamiltonians have significantly different ground state wavefunctions, due to hindered quantum tunneling through energy barriers [3]. Filtering methods such as quantum phase estimation [4, 5] and the rodeo algorithm [6] are probabilistic in nature. Their success probabilities are proportional to the initial state overlap with the eigenstate of interest, and these decrease exponentially with system size.

Despite these challenges, many quantum algorithms are indeed efficient and accurate when applied to systems restricted to a small model space, such as a limited number of single-particle orbitals or a coarse lattice grid. It would therefore be useful to have some means of bootstrapping these low-resolution eigenstates to produce the corresponding eigenstates for a larger model space. In this paper, we present a general approach called resolution refinement that performs this bootstrapping. The first step is to prepare an eigenstate of a low-resolution Hamiltonian using any method of choice. This is made possible because the model space is small. The eigenstate is then lifted to higher resolution and adiabatically evolved to produce the corresponding eigenstate of a higher-fidelity Hamiltonian. We show that many-body calculations using products of single-particle orbital states can be bootstrapped using basis refinement. We

also show that the resolution refinement can be applied to many-body lattice Hamiltonian simulations using lattice refinement.

Effective field theory and its implementation using renormalization group methods have been central to recent progress in nuclear theory using classical computation [7–17]. Resolution refinement can be viewed as a physics-inspired quantum computing algorithm based on principles of low-energy effective field theory and renormalization group flow. It acts like an inverse renormalization group transformation from low resolution to high resolution.

As a first example, we consider the Busch model [18] in one spatial dimension for K distinguishable fermions with mass m in a harmonic oscillator trap with angular frequency ω and same-strength delta function interactions between all pairs. We use harmonic oscillator units where length is in units of $\sqrt{\hbar/m\omega}$ and energy is in units of $\hbar\omega$. In the formalism of second quantization with creation and annihilation operators $a_{x,k}^\dagger$ and $a_{x,k}$, the Hamiltonian H has the form,

$$\frac{-1}{2} \sum_k \int dx a_{x,k}^\dagger \nabla^2 a_{x,k} + \frac{1}{2} \int dx [x^2 \rho_x + g : \rho_x^2 :], \quad (1)$$

where ρ_x is the local total density $\sum_k a_{x,k}^\dagger a_{x,k}$. The $::$ symbol denotes normal ordering, where annihilation operators are on the right and creation operators on the left. We use single-particle orbitals corresponding to harmonic oscillator eigenstates with quantum numbers $n = 0, \dots, n_{\max} - 1$, where n_{\max} is the basis truncation parameter. On a quantum computer, we assign one qubit to each of the $K n_{\max}$ modes.

We consider basis refinement calculations performed

at low resolution and $n_{\max} = 2$ and $n_{\max} = 10$. We let N be the total number of fermions. For $K = N = 2$, the ground state energy is known analytically [18], and the value is 1.3067 for coupling $g = 1$. At low resolution with $n_{\max} = 2$, the ground state energy is 1.3782. At high resolution with $n_{\max} = 10$, the energy is 1.3264. Let H_{low} be the low-resolution Hamiltonian for the $n_{\max} = 2$ truncation. We define a prolongation operator P that lifts every many-body basis state in the low-resolution space to the same many-body basis state in the $n_{\max} = 10$ high-resolution space. The restriction operator P^\dagger performs the projection from high-resolution space to the low-resolution space. Since P^\dagger has a large kernel mapped to zero, we will use an energy shift μ so that the low-energy states of interest will have energies below zero. This process can be implemented using first quantization with matrix quantum mechanics or second quantization with creation and annihilation operators.

The resolution refinement process consists of performing adiabatic evolution with time duration T from the shifted and prolonged low-resolution Hamiltonian $P(H_{\text{low}} - \mu)P^\dagger$ to the shifted high-resolution Hamiltonian $H_{\text{high}} - \mu$. We shift all the energies back by an amount μ afterwards. For all of the adiabatic evolution calculations in this work we use the interpolation functions $\cos^2[\theta(t)]$ and $\sin^2[\theta(t)]$ for the coefficients of $P(H_{\text{low}} - \mu)P^\dagger$ and $H_{\text{high}} - \mu$, respectively, with $\theta(t) = (\pi t)/(2T)$ and t ranging from 0 to T . This process is the same for basis refinement and for lattice refinement.

While resolution refinement can be applied to any low-energy eigenstate, we focus on ground state calculations in the present work. We can quantify the fidelity of resolution refinement by computing the overlap probability $|\langle \Psi_0 | \Phi(T) \rangle|^2$, where $|\Phi(T)\rangle$ is the final wavefunction after adiabatic evolution and $|\Psi_0\rangle$ is the ground state of H_{high} .

In Fig.1, we plot the ground state overlap probability versus total adiabatic evolution time T for $K = N = 2$, $K = N = 3$, and $K = N = 4$. For each case, the low-resolution calculation uses $n_{\max} = 2$ and the high-resolution calculation uses $n_{\max} = 10$. The energy gap, ΔE , for $K = N = 2$ is about 0.7. The energy gap is about 0.6 for $K = N = 3$ and about 0.5 for $K = N = 4$. We see that the overlap probabilities approach 1 with a timescale of $T \sim (\Delta E)^{-1}$. The convergence of adiabatic evolution is typically exponential at early times, but switches over to power law convergence at late times. As discussed in Ref. [19], it is therefore useful to combine adiabatic evolution with filtering algorithms such as the rodeo algorithm in order to have exponential convergence for late times also.

We now turn our attention to lattice refinement for lattice Hamiltonians. For lattice calculations on a quantum computer, we use the second quantization formalism with the occupation basis for each particle species, where $|0\rangle$ or $|1\rangle$ represents a particle of that species occupying

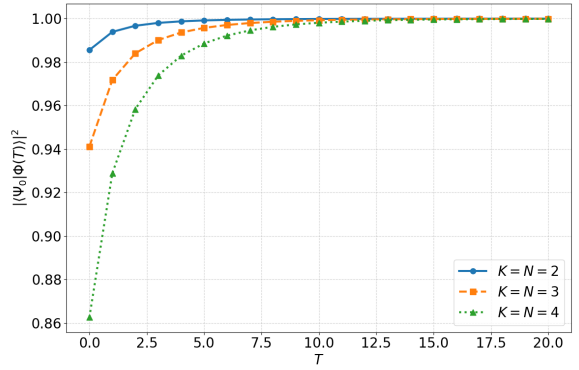


FIG. 1: Plot of the ground state overlap probabilities versus total adiabatic evolution time for $K = N = 2$, $K = N = 3$, and $K = N = 4$ for the Busch model in one dimensions.

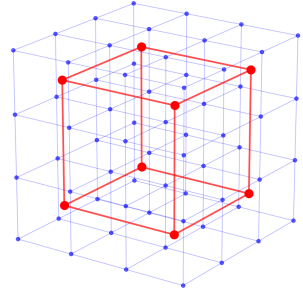


FIG. 2: Sketch of the fine lattice grid with spacing a and the coarse lattice grid with spacing $2a$.

a given lattice site or not. For lattice refinement we need a prolongation operator P that lifts many-body states on a coarse lattice with spacing $2a$ to the corresponding many-body states on a fine lattice grid with spacing a . The two lattice grids are illustrated in Fig. 2 for a three-dimensional lattice. Any operator at coarse lattice site $2\mathbf{r}$ becomes a normalized sum of operators at surrounding fine lattice sites $2\mathbf{r} \pm \hat{\mathbf{n}}/2$, where $\hat{\mathbf{n}}$ are lattice unit vectors along the d spatial directions.

To implement the prolongation operator on a quantum computer, we distribute any $|1\rangle$ state on a coarse lattice site to an equal superposition of 2^d states with exactly one $|1\rangle$ state on the surrounding fine lattice sites. For any $|0\rangle$ state on a coarse lattice site, we set all the surrounding fine lattice sites to $|0\rangle$. We first illustrate the process for one spatial dimension. For each qubit corresponding to a coarse lattice site, we introduce a second qubit initialized in the $|0\rangle$ state. We then apply a unitary operation U to these two qubits where $U|00\rangle = |00\rangle$ and $U|10\rangle = \frac{1}{\sqrt{2}}(|10\rangle + |01\rangle)$. Fig. 3 shows a simple

circuit that performs the required operations using two single-qubit rotations and two CNOT gates. This circuit

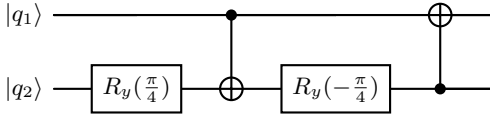


FIG. 3: The circuit decomposition for the unitary U operator built from single-qubit rotations and two CNOT gates.

provides the required prolongation along the x direction. For more than one spatial dimension, we simply apply the same process recursively for each spatial direction to the qubits obtained in the previous prolongation step.

For fermionic particles, we can choose a canonical ordering of modes such that each of the 2^d qubits are contiguous in the ordering. This convenient choice eliminates the need for keeping track of minus signs during the prolongation step. It is suitable for any lattice simulations of many-body fermions and hard core bosons. For lattice gauge theories, there are complications due to gauge fields residing on the lattice links as well as the Gauss' law constraints. The successful implementation of lattice refinement for gauge theories is beyond the scope of the present work.

For our benchmark lattice calculations, we consider a Hubbard model with K fermion species with mass m on a periodic cubic lattice in d spatial dimensions. We use natural units where \hbar and the speed of light, c , are set to 1. The Hamiltonian H has the form

$$\frac{-1}{2mb^2} \sum_{\langle \mathbf{r}, \mathbf{r}' \rangle, k} a_{\mathbf{r}, k}^\dagger a_{\mathbf{r}', k} + \sum_{\mathbf{r}, j < k} C_{j, k} \rho_{\mathbf{r}, j} \rho_{\mathbf{r}, k} + \sum_{\mathbf{r}, k} V_{\mathbf{r}} \rho_{\mathbf{r}, k}, \quad (2)$$

where b is the lattice spacing, $\langle \mathbf{r}, \mathbf{r}' \rangle$ denotes nearest neighbors, and $\rho_{\mathbf{r}, k}$ is the local density operator $a_{\mathbf{r}, k}^\dagger a_{\mathbf{r}, k}$ for species k . In the single-particle potential $V_{\mathbf{r}}$, we have included the term $d/(mb^2)$ needed to complete the finite-difference Laplacian in d dimensions. The parameters $C_{j, k}$ control the two-body interactions

For the first lattice benchmark, we set $C_{j, k} = 0$ and calculate Hartree-Fock lattice wavefunctions for a central Woods-Saxon potential of the form

$$V_{\mathbf{r}} = -\frac{V_0}{1 + e^{(|\mathbf{r}| - R)/\alpha}}, \quad R = R_0 A^{1/3}, \quad (3)$$

where A is the number of nucleons. The number of nucleon species is $K = 4$. For the fine lattice grid, we take $a = (150 \text{ MeV})^{-1} = 1.32 \text{ fm}$, matching recent nuclear lattice effective field theory calculations [20–27]. The coarse lattice grid then has lattice spacing $2a = (75 \text{ MeV})^{-1} = 2.63 \text{ fm}$. The nucleon mass is $m = 938.92 \text{ MeV}$, and the diffuseness parameter is taken to be $\alpha = 0.5 \text{ fm}$.

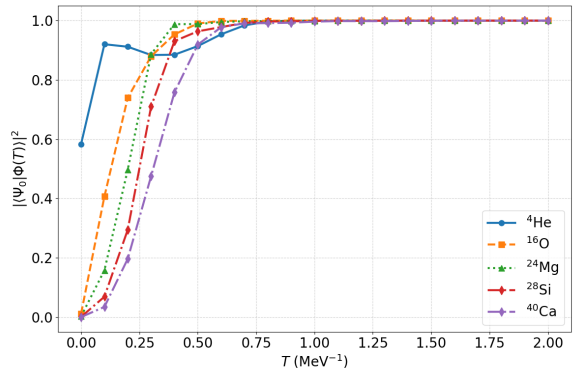


FIG. 4: Plot of the overlap probabilities versus total adiabatic evolution time for ${}^4\text{He}$, ${}^{16}\text{O}$, ${}^{24}\text{Mg}$, ${}^{28}\text{Si}$ and ${}^{40}\text{Ca}$.

For the depth V_0 and radius parameter R_0 , we adjust the parameters for the coarse and fine lattice Hamiltonians so that they produce similar energies and radii. We take $R_0 = 1.5 \text{ fm}$ and $V_0 = 50 \text{ MeV}$ for the fine lattice grid, and we take $R_0 = 1.8 \text{ fm}$ and $V_0 = 40 \text{ MeV}$ for the coarse lattice grid. For the lattice calculations, we need slightly larger values for R_0 in order to produce nuclear radii and binding energies similar to those obtained in continuous space.

We use lattice refinement to compute the ground state wavefunctions of ${}^4\text{He}$, ${}^{16}\text{O}$, ${}^{24}\text{Mg}$, ${}^{28}\text{Si}$, and ${}^{40}\text{Ca}$. For each of these calculations, the energy gap ΔE is between 10 and 15 MeV. In Fig. 4 we show the overlap probability $|\langle \Psi_0 | \Phi(T) \rangle|^2$ versus total evolution time T . We see that the overlap probability approaches 1 with a timescale comparable to $(\Delta E)^{-1}$. For ${}^{40}\text{Ca}$, the overlap probability starts at 8×10^{-6} and rises by five orders of magnitude. For ${}^4\text{He}$ there are some oscillations as often happens in adiabatic evolution. This performance can be improved by using adiabatic evolution for $T \approx 0.1 \text{ MeV}^{-1}$ and then switching to a filtering method such as the rodeo algorithm to get exponential convergence of the overlap probability at later times. The fact that the lattice refinement is not producing any difficulties can be seen by plotting the energy levels for H_λ , which linearly interpolates between $P(H_{\text{low}} - \mu)P^\dagger + \mu$ at $\lambda = 0$ and H_{high} at $\lambda = 1$. In Fig. 5, we plot the single-particle energy levels for H_λ for one nucleon species in ${}^{40}\text{Ca}$. We have labeled the corresponding irreducible cubic representations. We see that the curves are very smooth, making the adiabatic evolution efficient.

For our last benchmark calculation, we compute the five-body bound states and continuum states for $K = 5$ distinguishable fermions in the one-dimensional Hubbard model. We again take the fermion masses to be $m = 938.92 \text{ MeV}$, and we take $V_{\mathbf{r}}$ to contain the Laplacian term only, $1/(mb^2)$. In Table I, we show the two-body interaction coefficients used to produce cluster ground

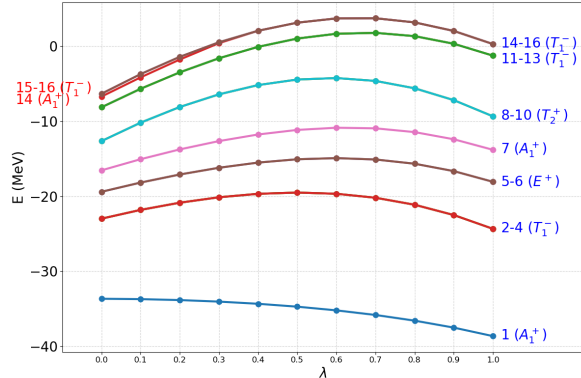


FIG. 5: Single-particle energy levels for one nucleon species for the ^{40}Ca calculation as function of interpolation parameter λ . We have labeled the corresponding irreducible cubic representations.

states with $1 + 1 + 1 + 1 + 1$, $2 + 1 + 1 + 1$, $2 + 2 + 1$, $3 + 1 + 1$, $3 + 2$, $4 + 1$, and 5 particles.

TABLE I: Two-body interaction coefficients producing the various cluster ground states.

state	$C_{j,k} = -20$ MeV	$C_{j,k} = 10$ MeV	$C_{j,k} = 20$ MeV
$1+1+1+1$		$(1,5), (2,3), (3,5), (4,5)$	$(1,2), (2,4), (3,4)$
$+1+1$			
$2+1+1+1$	$(1,2)$	$(1,5), (2,3), (3,5), (4,5)$	$(2,4), (3,4)$
$+1$			
$2+2+1+1$	$(1,2), (3,4)$	$(1,5), (2,3), (3,5), (4,5)$	$(2,4)$
$+1$			
$3+1+1+1$	$(1,2), (2,3)$	$(1,5)$	$(2,4)$
$+1$			
$3+2$	$(1,2), (2,3), (4,5)$		$(2,4)$
$4+1$	$(1,2), (2,3), (2,4)$		$(4,5)$
5	$(1,2), (2,3), (2,4), (4,5)$		

In Fig. 6 we show the overlap probability $|\langle \Psi_0 | \Phi(T) \rangle|^2$ versus total evolution time T for the various one-dimensional Hubbard model Hamiltonians corresponding to the interaction coefficients in Table I. If we do not count excited states that are translational modes of the ground states, the energy gap ΔE for each Hamiltonian considered is about 4 or 5 MeV. As found before, the overlap probability approaches 1 with a timescale comparable to $(\Delta E)^{-1}$. There are again oscillations at later times, but as before we can limit adiabatic evolution to $T \approx 0.25$ MeV $^{-1}$ and switch to a filtering method to complete the state preparation.

In this work, we have presented a technique called resolution refinement that allows one to bootstrap eigenstate preparation. We start with an eigenstate of a low-resolution Hamiltonian and lift the eigenstate to a high-resolution space. Adiabatic evolution is then used to

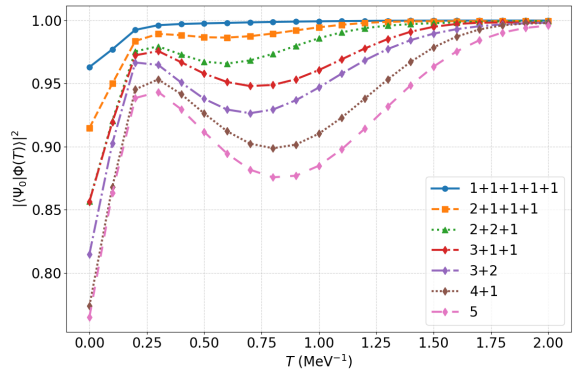


FIG. 6: Ground state overlap probability for cluster states composed of $1 + 1 + 1 + 1 + 1$, $2 + 1 + 1 + 1$, $2 + 2 + 1$, $3 + 1 + 1$, $3 + 2$, $4 + 1$, and 5 particles for various one-dimensional Hubbard model Hamiltonians. We plot $|\langle \Psi_0 | \Phi(T) \rangle|^2$ versus total adiabatic evolution time T .

prepare the corresponding eigenstate of a high-resolution Hamiltonian. Filtering methods can be used to augment the performance of adiabatic evolution. We have presented benchmark examples for basis refinement as well as lattice refinement. In all cases, the adiabatic evolution time required is comparable to the inverse of the energy gap in the physical spectrum. Resolution refinement is a general purpose and practical approach based on the principles of effective field theory that can be used to extend the reach of currently used many-body state preparation methods. While the method may fail for systems that are extremely large or manifest correlations that are not properly captured by the low-resolution Hamiltonian, it appears broadly useful for a wide range of quantum many-body problems.

We acknowledge financial support from the U.S. Department of Energy through grants DE-SC0023658, DE-SC0013365, DE-SC0024586, DE-SC0023175, DE-SC0026198, DE-SC0023516, and the U.S. National Science Foundation through grants PHY-2310620 and PHY-2310020. This research used resources of the Oak Ridge Leadership Computing Facility, which is a DOE Office of Science User Facility supported under contract DE-AC05-00OR22725.

- [1] A. Peruzzo, J. McClean, P. Shadbolt, M.-H. Yung, X.-Q. Zhou, P. J. Love, A. Aspuru-Guzik, and J. L. O’brien, Nat. Commun. **5**, 4213 (2014).
- [2] J. R. McClean, S. Boixo, V. N. Smelyanskiy, R. Babbush, and H. Neven, Nat. Commun. **9**, 4812 (2018).
- [3] T. Albash and D. A. Lidar, Reviews of Modern Physics **90**, 015002 (2018).
- [4] A. Y. Kitaev, arXiv preprint quant-ph/9511026 (1995).

[5] D. S. Abrams and S. Lloyd, Phys. Rev. Lett. **83**, 5162 (1999).

[6] K. Choi, D. Lee, J. Bonitati, Z. Qian, and J. Watkins, (2020), arXiv:2009.04092 [quant-ph].

[7] S. Bogner, T. T. S. Kuo, L. Coraggio, A. Covello, and N. Itaco, Phys. Rev. C **65**, 051301 (2002), arXiv:nucl-th/9912056.

[8] S. K. Bogner, R. J. Furnstahl, and R. J. Perry, Phys. Rev. C **75**, 061001 (2007), arXiv:nucl-th/0611045.

[9] K. Tsukiyama, S. K. Bogner, and A. Schwenk, Phys. Rev. Lett. **106**, 222502 (2011), arXiv:1006.3639 [nucl-th].

[10] H. Hergert, S. K. Bogner, S. Binder, A. Calci, J. Langhammer, R. Roth, and A. Schwenk, Phys. Rev. C **87**, 034307 (2013), arXiv:1212.1190 [nucl-th].

[11] N. Tsunoda, K. Takayanagi, M. Hjorth-Jensen, and T. Otsuka, Phys. Rev. C **89**, 024313 (2014), arXiv:1310.7107 [nucl-th].

[12] G. Hagen *et al.*, Nat. Phys. **12**, 186 (2015), arXiv:1509.07169 [nucl-th].

[13] A. Ekström, G. R. Jansen, K. A. Wendt, G. Hagen, T. Papenbrock, B. D. Carlsson, C. Forssén, M. Hjorth-Jensen, P. Navrátil, and W. Nazarewicz, Phys. Rev. C **91**, 051301 (2015), arXiv:1502.04682 [nucl-th].

[14] S. Elhatisari *et al.*, Phys. Rev. Lett. **117**, 132501 (2016), arXiv:1602.04539 [nucl-th].

[15] S. R. Stroberg, A. Calci, H. Hergert, J. D. Holt, S. K. Bogner, R. Roth, and A. Schwenk, Phys. Rev. Lett. **118**, 032502 (2017), arXiv:1607.03229 [nucl-th].

[16] J. M. Yao, B. Bally, J. Engel, R. Wirth, T. R. Rodríguez, and H. Hergert, Phys. Rev. Lett. **124**, 232501 (2020), arXiv:1908.05424 [nucl-th].

[17] D. Lee *et al.*, (2020), arXiv:2010.09420 [nucl-th].

[18] T. Busch, B.-G. Englert, K. Rzażewski, and M. Wilkens, Foundations of Physics **28**, 549 (1998).

[19] M. Patkowski, O. Ayyildiz, M. Kebrič, K. L. C. Hunt, and D. Lee, (2025), arXiv:2510.19039 [quant-ph].

[20] B.-N. Lu, N. Li, S. Elhatisari, Y.-Z. Ma, D. Lee, and U.-G. Meißner, Phys. Rev. Lett. **128**, 242501 (2022), arXiv:2111.14191 [nucl-th].

[21] S. Shen, S. Elhatisari, T. A. Lähde, D. Lee, B.-N. Lu, and U.-G. Meißner, Nature Commun. **14**, 2777 (2023), arXiv:2202.13596 [nucl-th].

[22] S. Elhatisari *et al.*, Nature **630**, 59 (2024), arXiv:2210.17488 [nucl-th].

[23] Y.-Z. Ma, Z. Lin, B.-N. Lu, S. Elhatisari, D. Lee, N. Li, U.-G. Meißner, A. W. Steiner, and Q. Wang, Phys. Rev. Lett. **132**, 232502 (2024), arXiv:2306.04500 [nucl-th].

[24] U.-G. Meißner, S. Shen, S. Elhatisari, and D. Lee, Phys. Rev. Lett. **132**, 062501 (2024), arXiv:2309.01558 [nucl-th].

[25] G. Giacalone *et al.*, Phys. Rev. Lett. **135**, 012302 (2025), arXiv:2402.05995 [nucl-th].

[26] G. Giacalone *et al.*, Phys. Rev. Lett. **134**, 082301 (2025), arXiv:2405.20210 [nucl-th].

[27] K. König *et al.*, Phys. Rev. Lett. **132**, 162502 (2024), [Erratum: Phys. Rev. Lett. 133, 059901 (2024)], arXiv:2309.02037 [nucl-ex].